ChemComm

Extension of the mechanoresponsive luminescence shift via formation of a doped organic crystal

Journal:	*ChemComm*
Manuscript ID	CC-COM-02-2022-000741.R2
Article Type:	Communication

ChemComm

COMMUNICATION

Extension of the mechanoresponsive luminescence shift via formation of a doped organic crystal

Ryohei Yoshida,[a] Takashi Tachikawa*[b,c] and Suguru Ito*[a,d]

Received 00th January 20xx,
Accepted 00th January 20xx

DOI: 10.1039/x0xx00000x

Herein, we propose a new strategy to tune the magnitude of mechanoresponsive shift of the maximum emission wavelength ($\Delta\lambda_{em}$). The $\Delta\lambda_{em}$ of thienylbenzothiadiazole crystals has been extended to 69 nm by doping a trace amount of dithienylbenzothiadiazole, whereas the pure crystal of thienylbenzothiadiazole exhibited the $\Delta\lambda_{em}$ of 10 nm. This doping strategy should accelerate the development of advanced mechanosensing materials composed of organic crystals.

The past decade has witnessed a remarkable surge in luminescent organic crystals, and particular interest has focused on their mechanochromic luminescence (MCL).[1] A considerable number of organic MCL crystals that can switch photoluminescence properties in response to mechanical stimuli have been developed owing to the wealth of promising applications in pressure sensors, anticounterfeiting inks, etc. The emission wavelength of typical organic MCL crystals shifts in the bathochromic direction upon grinding, whereas relatively few are known to show the mechano-induced hypsochromic shift of the emission.[2] Although the emission wavelength shifts are usually rationalized by the difference in molecular conformations and arrangements between initial and mechanically generated states,[3] the rational tuning of the mechano-induced shift remains an outstanding challenge. Establishing a reliable method to control the direction and magnitude of the wavelength shift is of great importance from the academic perspective and practical applications of organic MCL crystals.

A promising method to control the photoluminescence properties of organic crystals is to prepare two-component materials by mixing a luminescent compound with another compound.[4] Cocrystals[5b,c,g] or segregated crystals[5a,d,e] prepared by this method often exhibit remarkable MCL compared with crystals composed of the single luminescent compound. These two-component crystals have advantages over single-component crystals, which require the modification of molecular structures[6a] or the incidental formation of polymorphic crystals[6b] to tune the mechanoresponsive properties. On the other hand, the reported two-component crystals require stoichiometric amounts of each compound.

Organic solid solutions, or mixed crystals, are characterized by the structural disorder of the host crystal, which contains varying amounts of guest molecules in the crystal lattice and exhibits variable physicochemical properties.[7] Luminescence properties can be tuned by forming mixed crystals with subequimolar amounts of guest compounds.[8] Moreover, a trace amount of dopant molecules can often significantly change the emission colors and lifetimes of luminescent mixed crystals.[9] Nevertheless, such a doping strategy has been unexplored to control the mechanoresponsive properties of luminescent organic crystals.

We have recently reported the versatile MCL properties of donor-acceptor-type benzothiadiazole derivatives.[2a,c,10] Among these, 4-(2-thienyl)-2,1,3-benzothiadiazole (**1**) showed a relatively small shift in the maximum emission wavelength upon grinding (Fig. 1a).[2a] Specifically, the plate-like crystals of **1** showed a blue-green fluorescence at the maximum emission wavelength (λ_{em}) of 502 nm with the good fluorescence quantum yield (Φ_F) of 0.64. Upon grinding with a spatula, the emission wavelength of **1** was shifted by 10 nm in the hypsochromic direction to show a light-blue emission (λ_{em} = 492 nm, Φ_F = 0.54).

Herein, we report the control over the mechanoresponsive luminescence of crystalline **1** by doping a trace amount of 4,7-di(2-thienyl)benzothiadiazole **2** (Fig. 1b). Most remarkably, the mechanoresponsive shift in the maximum emission wavelength ($\Delta\lambda_{em}$) has been extended from 10 nm to 69 nm by preparing the doped mixed crystals **1•2**. Mechanistic studies have revealed that the mechanoresponsive on/off switching of the Förster resonance energy transfer (FRET) from **1** to **2** should contribute to the larger $\Delta\lambda_{em}$ of the doped mixed crystals **1•2** compared with the single-component crystals of **1**.

[a] *Department of Chemistry and Life Science, Graduate School of Engineering Science, Yokohama National University, 79-5 Tokiwadai, Hodogaya-ku, Yokohama 240-8501, Japan. E-mail: suguru-ito@ynu.ac.jp*
[b] *Department of Chemistry, Graduate School of Science, Kobe University, 1-1 Rokkodai-cho, Nada-ku, Kobe 657-8501, Japan*
[c] *Molecular Photoscience Research Center, Kobe University, 1-1 Rokkodai-cho, Nada-ku, Kobe 657-8501, Japan. E-mail: tachikawa@port.kobe-u.ac.jp*
[d] *PRESTO, Japan Science and Technology Agency (JST), 4-1-8 Honcho, Kawaguchi, Saitama 332-0012, Japan.*

†Electronic Supplementary Information (ESI) available: Experimental details, single-crystal X-ray structures, spectral data, PXRD analyses, DSC thermograms, and fluorescence lifetimes.

Plate-like mixed crystals **1•2** were obtained by recrystallization from cyclohexane solution of **1** containing a trace amount (250 ppm) of **2**. The color of the crystals **1•2** was yellow under room light, which was different from the pale yellow crystals **1**[2a] and red

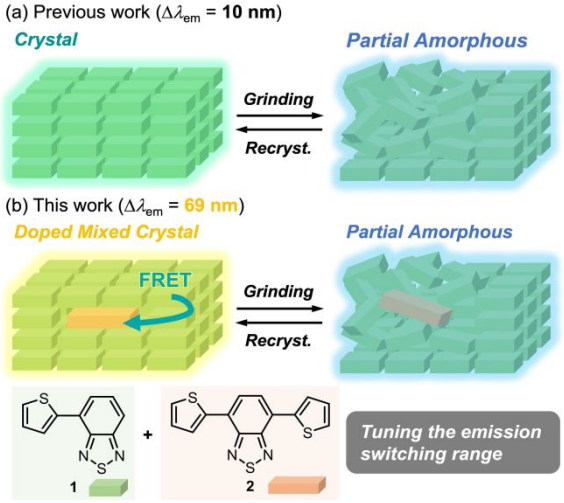

Fig. 1 Schematic illustration for the mechanoresponsive emission-color switching between crystalline and partially amorphous states. (a) Previous work: Thienylbenzothiadiazole **1** with $\Delta\lambda_{em}$ of 10 nm. (b) This work: Doped mixed crystals of **1** and **2** with $\Delta\lambda_{em}$ of 69 nm.

crystals **2**[11] (Fig. 2a). On the basis of HPLC analysis, the amount of **2** included in the mixed crystals **1•2** was (3.7±1.6) × 10^2 ppm (Table S1). The powder X-ray diffraction (PXRD) analysis indicated that the crystal system of the yellow crystals **1•2** is the same as that of the single-component crystals of **1** (Fig. 2b). Accordingly, a trace amount of **1** in the crystal structure should be replaced by **2** to form the doped mixed crystals **1•2**. Although **2** is larger than **1**, the adjacent two molecules of **1** in the crystal structure would be replaced by a single molecule of **2** (Fig. S1).

In the absorption spectrum of crystalline **1•2** obtained by measuring the diffuse reflectance spectrum after diluted in $BaSO_4$, a new band was observed at around 500 nm which would be attributed to the absorption of **2** rather than charge-transfer transitions from **1** to **2** (Fig. 2c, S1 and S3). Although only trace **2** was doped into the crystal, the absorption of **2** was observed in the spectrum. This is because the absorption by trace **2** should continuously occur while the light passes over long paths in the interior of the transparent crystals. Moreover, the mixed crystals **1•2** exhibited a yellow fluorescence which was different from the blue-green emission of crystalline **1** and red emission of crystalline **2** (Fig. 2a). In the emission spectrum of crystalline **1•2**, the emission maximum was observed at 559 nm with a shoulder band at around 500 nm (Fig. 2d).

The mixed crystals **1•2** exhibited a more prominent shift in the emission wavelength upon mechanical stimulation compared with the crystals consisting only of **1**. Upon grinding with a spatula (40–70 N cm^{-2}), the yellow emission (λ_{em} = 559 nm, Φ_F = 0.58) of crystalline **1•2** shifted hypsochromically to the light blue emission (λ_{em} = 490 nm, Φ_F = 0.54) (Fig. 3a, 3b, and S7 and Table S2). Namely, the $\Delta\lambda_{em}$ between the crystalline and ground states could be extended from 10 nm in **1** (Fig. S2) to 69 nm by forming the mixed crystals with **2**. The PXRD peaks of crystalline **1•2** were still observed after grinding, although the intensity of peaks was reduced compared with that of the initial crystalline state (Fig. S5). In contrast to typical MCL compounds, the original yellow emission was not recovered after heating the ground **1•2** to 60 °C.

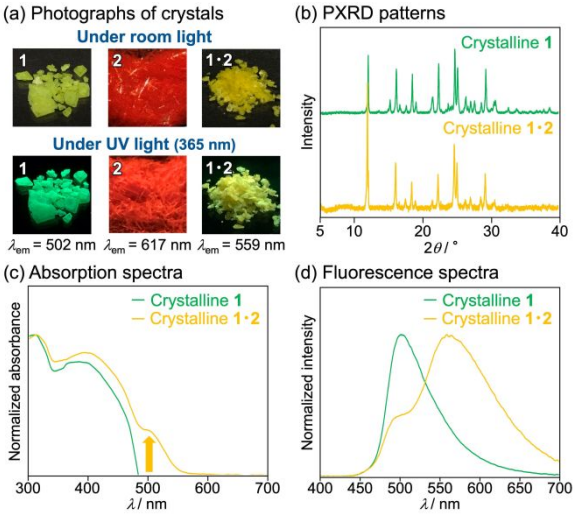

Fig. 2 (a) Photographs of crystals of **1**, **2**, and **1•2** under room light and UV light (365 nm). (b) PXRD patterns, (c) absorption spectra, (d) and fluorescence spectra (λ_{ex} = 365 nm) of crystalline **1** and **1•2**.

Recrystallization from cyclohexane was required to recover the initial crystalline **1•2** from the ground state. The DSC thermograms of **1•2** showed only one endothermic peak corresponding to the melting point at 68 ℃ for both crystalline and ground samples, which were almost identical to those of **1** (Fig. S6). On the basis of the endothermic DSC peaks, the enthalpy values of the melting points were −20.5 kJ/mol and −18.2 kJ/mol for initial and ground **1•2**, respectively. These results indicate that only the partial decomposition of the crystal structures could induce the remarkable hypsochromic shift in the emission wavelength of **1•2** in response to mechanical stimuli.

The absorption and emission bands of ground **1•2** should mainly be originated from ground **1**. The fluorescence spectrum of ground **1•2** was in good agreement with that of ground **1**, although a shoulder band was observed for ground **1•2** at around 550 nm (Fig. 3b). Meanwhile, the intensity of the absorption band of crystalline **1•2** at around 500 nm significantly decreased after grinding because the light scattering efficiency was improved by grinding the

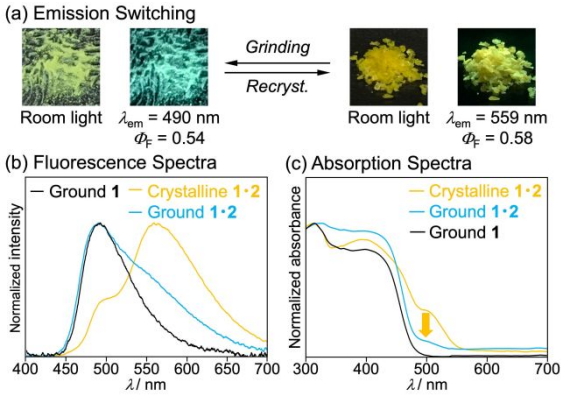

Fig. 3 (a) Photographs of crystalline and ground **1•2** under room light and UV (365 nm) light. (b) Fluorescence spectra of crystalline **1•2**, ground **1•2**, and ground **1** (λ_{ex} = 365 nm). (c) Absorption spectra of crystalline **1•2**, ground **1•2**, and ground **1**.

transparent crystals into fine powders, and the resulting spectrum was

almost identical to that of ground **1** (Fig. 3c).

The optimal amount of **2** to be mixed in preparing doped crystals was 250 ppm for magnifying the degree of mechanoresponsive shift in emission wavelength. Recrystallization from a cyclohexane solution of an equimolar amount of **1** and **2** afforded crystals of **2** due to the lower solubility of **2**. When a cyclohexane solution of **1** containing 1000 ppm of **2** was used, the intensity of the new absorption band at around 500 nm was larger for the cultivated mixed crystals **1•2** (1000 ppm) than that of **1•2** prepared by doping with a smaller amount (250 ppm) of **2** (Fig. S3). Moreover, the emission band of **1•2** (1000 ppm) was observed in the bathochromic region (λ_{em} = 575 nm, Fig. S2) compared with that of **1•2** (250 ppm) (λ_{em} = 559 nm, Fig. 3). However, the emission maximum of **1•2** (1000 ppm) showed a small shift ($\Delta\lambda_{em}$ = 14 nm) after grinding, and a slight increase in the peak intensity at around 500 nm was observed for the fluorescence spectrum of the ground sample (Fig. S2).

Spatially resolved fluorescence microscopy revealed that the bulk sample of mixed crystals **1•2** (250 ppm) contains both yellow-emissive crystals (ca. 1 mm square) and blue-green-emissive microcrystals (ca. 5–15 μm square) (Fig. 4a). The observation of a yellow-emissive crystal showed that the large areas of the crystal surface exhibited yellow emission peaking at 582 nm (Fig. 4b, yellow line), and some small areas of blue-green emission were also observed (Fig. 4a). The maximum emission wavelength of blue- green-emissive microcrystals was 507 nm (Fig. 4a inset and Fig. 4b, blue-green line), which was in good agreement with that of crystalline **1** (Fig. 2a). These results suggest that microcrystals of **1** were also formed from the solution of **1** with 250 ppm of **2**, and the fluorescence spectrum observed in the bulk sample of **1•2** (250 ppm)

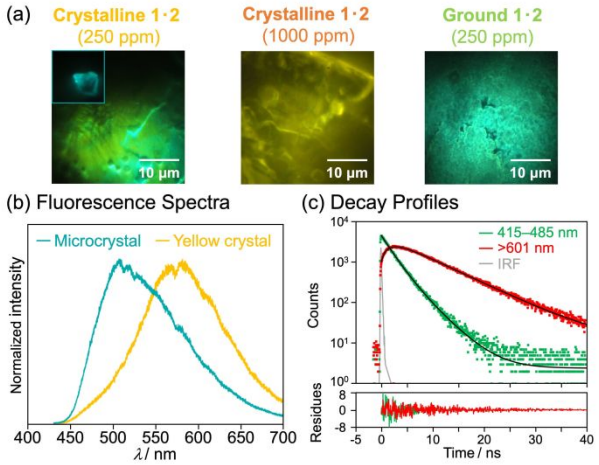

Fig. 4 Fluorescence microscopy of **1•2** (λ_{ex} = 405 nm). (a) Photographs of a yellow-emissive crystal and a blue-green-emissive microcrystal (inset) contained in crystalline **1•2** (250 ppm) (left), crystalline **1•2** (1000 ppm) (center), and ground **1•2** (250 ppm) (right). The square marks indicate the measured locations of fluorescence spectra and fluorescence decay profiles. (b) Fluorescence spectra of a blue-green-emissive microcrystal (blue-green line) and a yellow-emissive crystal (yellow line) contained in crystalline **1•2** (250 ppm). (c) Fluorescence decay profiles of a yellow-emissive crystalline **1•2** (250 ppm) monitored at 415–485 nm (green squares) and > 601 nm (red squares). The black lines indicate multi-exponential curves fitted to the time profiles. The grey line indicates the instrument response function (IRF).

Table 1 Fluorescence decay and rise times for crystalline **1•2** (250 ppm), crystalline **1•2** (1000 ppm), and ground **1•2** (250 ppm) in the short- and long-wavelength regions.

Sample	Region (nm)	τ_1[a] (ns)	τ_2[a] (ns)
Crystalline **1•2** (250 ppm)	415–485	2.0 (0.61)	3.7 (0.39)
	> 601	1.8 (–0.25)	7.3 (1.25)
Crystalline **1•2** (1000 ppm)	415–485	1.0 (0.66)	2.8 (0.34)
	> 601	0.9 (–0.08)	7.7 (1.08)
Ground **1•2** (250 ppm)	415–485	2.5 (0.23)	6.2 (0.77)
	> 601	2.1 (–0.18)	8.4 (1.18)

[a] The fractional contribution f_n of the component is indicated in parentheses.

corresponds to the sum of the emission from the yellow-emissive mixed crystals **1•2** and the blue-green-emissive microcrystals **1**. The emission maximum of crystalline **1•2** (250 ppm) in the bulk state was observed in the hypsochromic region (λ_{em} = 559 nm) compared with that of the yellow-emissive surface observed in the fluorescence microscopy (λ_{em} = 582 nm). This deviation can be explained by the fact that the fluorescence spectrum in the bulk **1•2** contains the emission from crystalline **1** in the short-wavelength region.

The fluorescence decay analyses revealed that the energy transfer from **1** to **2** occurred in the mixed crystals. The new absorption band observed for mixed crystals **1•2** at around 500 nm (Fig. 2c) should overlap well with the blue-green emission of crystalline **1** (Fig. 2a and S2), which is the prerequisite for the FRET process.[12] The excitation spectrum of crystalline **1•2** (250 ppm) was in good agreement with its absorption spectrum, with a relatively intense band around 500 nm (Fig. S4). The fluorescence decay profiles of crystalline **1•2** (250 ppm) were monitored in the short-wavelength region (415–485 nm) and long-wavelength region (> 601 nm) using bandpass filters (Fig. 4c, S8 and Table 1). The observed emission in the short- and long-wavelength regions should correspond to the emission from **1** and **2**, respectively. The lifetime decay curve in the short-wavelength region fitted well to double-exponential functions (Fig. 4c, green squares). The lifetimes of short-lived (τ_1) and long-lived components (τ_2) were 2.0 ns and 3.7 ns, respectively. Meanwhile, the emission lifetime of crystalline **1** was 7.2 ns (Table S2 and Fig. S9). Namely, the lifetime of the emission from **1** significantly decreased in the mixed crystal. On the other hand, a rise component was observed in the long-wavelength region (Fig. 4c, red squares). The rise time (τ_1) was 1.8 ns, which was in good agreement with the fast decay time (τ_1 = 2.0 ns) observed in the short-wavelength emission. These results indicate that the FRET from **1** to **2** should occur in the mixed crystals.

Mixed crystals **1•2** (1000 ppm) exhibited a faster FRET than **1•2** (250 ppm). When **1•2** (1000 ppm) was observed via fluorescence microscopy, almost the entire crystal surface showed yellow emission (λ_{em} = 583 nm, Fig. 4a and S10). In this yellow-emissive region, the rise time (τ_1 = 0.9 ns) of the long-wavelength emission, which is identical to the fast decay time (τ_1 = 1.0 ns) of the short-wavelength emission, is shorter than that of mixed crystals (250 ppm) (Table 1). Therefore, the FRET process from **1** to **2** should be accelerated in the mixed crystals containing a larger number of energy acceptor **2**.

The FRET efficiency was significantly decreased after grinding the mixed crystals **1•2** (250 ppm), which should account for the pronounced hypsochromic shift of the emission wavelength. Spatially resolved fluorescence microscopy of ground **1•2** (250 ppm) showed

the almost homogeneous blue-green emission (λ_{em} = 518 nm) from the entire sample (Fig. 4a and S11). Although the rise component (τ_1 = 2.1 ns) was observed in the long-wavelength emission (> 601 nm) of ground **1•2** (250 ppm), the contribution of this FRET emission to the total emission (> 425 nm) was trivial. In the short-wavelength region (415–485 nm) of ground **1•2** (250 ppm), the fluorescence lifetime and fractional contribution of τ_2 component increased significantly (τ_2 = 6.2 ns, f_2 = 0.77, Table 1) compared with those observed in crystalline **1•2** (τ_2 = 3.7 ns, f_2 = 0.39, Table 1). Moreover, the τ_2 value of ground **1•2** (250 ppm) is close to the fluorescence lifetime of ground **1** (τ = 6.9 ns, Table S2 and Fig. S9). These results support that the fluorescence spectrum of ground **1•2** (250 ppm) is mainly attributed to the light-blue emission of ground **1**. In the ground **1•2**, the FRET efficiency should be decreased due to the partial formation of amorphous **1** in the crystal structure.

In summary, the mechanoresponsive luminescence of thienylbenzothiadiazole **1** could be tuned by forming mixed crystals with a trace amount of dithienylbenzothiadiazole **2**. The maximum emission wavelength of doped mixed crystals **1•2** shifted bathochromically in comparison with that of crystalline **1**. Consequently, the mechanoresponsive hypsochromic shift of the emission wavelength ($\Delta\lambda_{em}$) was extended from 10 nm for **1** to 69 nm for **1•2**. The emission decay analyses via fluorescence microscopy revealed that the large $\Delta\lambda_{em}$ of **1•2** should be attributed to the drastic decrease in the FRET efficiency from **1** to **2** after grinding. The doped crystal principle to control the $\Delta\lambda_{em}$ range should not be limited to the combinations presented. Other doped organic crystals with desirable mechanoresponsive properties can be expected to emerge in the near future, which should facilitate the development of advanced sensor systems that can detect mechanical stimuli as a distinct emission-color switching.

This work was partly supported by JSPS KAKENHI Grant Number JP20K05645 within the Grant-in-Aid for Scientific Research (C), JSPS KAKENHI Grant Numbers JP20H04665 and JP20H04673 within the Grant-in-Aid for Scientific Research on Innovative Areas "Soft Crystals: Area No. 2903", and JST, PRESTO Grant Number JPMJPR21A3, Japan. Part of this work was carried out by the joint research program Numbers R02019 and R03007 of Molecular Photoscience Research Center, Kobe University.

Conflicts of interest

There are no conflicts to declare.

Notes and references

1 For reviews, see: (a) S. Ito, *Chem. Lett.*, 2021, **50**, 649; (b) M. Kato, H. Ito, M. Hasegawa and K. Ishii, *Chem. - Eur. J.*, 2019, **25**, 5105; (c) Y. Sagara, S. Yamane, M. Mitani, C. Weder and T. Kato, *Adv. Mater.*, 2016, **28**, 1073.

2 For examples, see; (a) R. Yoshida, T. Tachikawa and S. Ito, *Cryst. Growth Des.*, 2022, **22**, 547; (b) H.-W. Zheng, S. Li, M. Wu, Y. Kang, J.-B. Li, Q.-F. Liang, X.-J. Zheng, D.-C. Fang and L.-P. Jin, *J. Mater. Chem. C*, 2020, **8**, 4246; (c) S. Nagai, M. Yamashita, T. Tachikawa, T. Ubukata, M. Asami and S. Ito, *J. Mater. Chem. C*, 2019, **7**, 4988; (d) A. Adak, T. Panda, A. Raveendran, K. S. Bejoymohandas, K. S. Asha, A. P. Prakasham, B. Mukhopadhyay and M. K. Panda, *ACS Omega*, 2018, **3**, 5291; (e) Y. Liu, Q. Zeng, B. Zou, Y. Liu, B. Xu and W. Tian, *Angew. Chem., Int. Ed.*, 2018, **57**, 15670; (f) T. Seki, K. Kobayashi, T. Mashimo and H. Ito, *Chem. Commun.*, 2018, **54**, 11136.

3 S. Ito, *J. Photochem. Photobiol., C*, 2022, **51**, 100481.

4 For reviews, see: (a) X. Deng, X. Yu, J. Xiao, Q. Zhang, *Aggregate*, 2021, **2**, e35; (b) Y. Huang, Z. Wang, Z. Chen, Q. Zhang, *Angew. Chem., Int. Ed.* 2019, **58**, 9696.

5 For recent examples of two-component MCL materials, see: (a) S. Ito, R. Sekine, M. Munakata, M. Yamashita and T. Tachikawa, *Chem. - Eur. J.*, 2021, **27**, 13982; (b) J.-J. Liu, S.-B. Xia, T. Liu, J.-M. Liu and F.-X. Cheng, *CrystEngComm*, 2021, **23**, 4320; (c) Z. Wang, F. Yu, W. Chen, J. Wang, J. Liu, C. Yao, J. Zhao, H. Dong, W. Hu and Q. Zhang, *Angew. Chem., Int. Ed.*, 2020, **59**, 17580; (d) M. Ikeya, G. Katada and S. Ito, *Chem. Commun.,* 2019, **55**, 12296; (e) S. Ito, G. Katada, T. Taguchi, I. Kawamura, T. Ubukata and M. Asami, *CrystEngComm*, 2019, **21**, 53; (f) Z. Ma, Y. Ji, Z. Wang, G. Kuang and X. Jia, *J. Mater. Chem. C*, 2016, **4**, 10914.

6 (a) X. Huang, L. Qian, Y. Zhou, M. Liu, Y. Cheng and H. Wu, *J. Mater. Chem. C*, 2018, **6**, 5075; (b) S. Ito, *CrystEngComm*, 2022, **24**, 1112.

7 (a) M. Lusi, *CrystEngComm*, 2018, **20**, 7042; (b) M. Lusi, *Cryst. Growth Des.*, 2018, **18**, 3704. (c) A. R. West, *Basic Solid State Chemistry, 2nd Edition;* John Wiley & Sons, Ltd.: Chichester, U.K., 1999.

8 (a) R. Thomas, S. P. Thomas, H. Lakhotiya, A. H. Mamakhel, M. Bondesgaard, V. Birkedal and B. B. Iversen, *Chem. Sci.*, 2021, **12**, 12391; (b) T. Seki, N. Toyoshima and H. Ito, *Dalton Trans.*, 2020, **49**, 2073; (c) C.-R. Wang, Y.-Y. Gong, W.-Z. Yuan and Y.-M. Zhang, *Chin. Chem. Lett.*, 2016, **27**, 1184; (d) O. Bolton, D. Lee, J. Jung and J. Kim, *Chem. Mater.*, 2014, **26**, 6644; (e) D. Yan and D. G. Evans, *Mater. Horiz.*, 2014, **1**, 46; (f) H. Li, L. Duan, D. Zhang, G. Dong, L. Wang and Y. Qiu, *J. Cryst. Growth*, 2008, **310**, 2537.

9 (a) D. Y. Muleta, J. Song, W. Feng, R. Wu, X. Zhou, W. Li, L. Wang, D. Liu, T. Wang and W. Hu, *J. Mater. Chem. C*, 2021, **9**, 5093; (b) J. Song, D. Y. Muleta, W. Feng, Y. Song, X. Zhou, W. Li, L. Wang, D. Liu, T. Wang and W. Hu, *Dyes Pigm.*, 2021, **193**, 109501; (c) S. Cui, Y. Liu, G. Li, Q. Han, C. Ge, L. Zhang, Q. Guo, X. Ye and X. Tao, *Cryst. Growth Des.*, 2020, **20**, 783; (d) J. Han, W. Feng, D. Y. Muleta, C. N. Bridgmohan, Y. Dang, G. Xie, H. Zhang, X. Zhou, W. Li, L. Wang, D. Liu, Y. Dang, T. Wang and W. Hu, *Adv. Funct. Mater.*, 2019, **29**, 1902503; (e) Y. Zhao, X. Wang, M. Li, B. Zhang and H. Wang, *Synth. Met.*, 2017, **223**, 12; (f) L. Xiao, Y. Wu, J. Chen, Z. Yu, Y. Liu, J. Yao and H. Fu, *J. Phys. Chem. A*, 2017, **121**, 8652.

10 (a) S. Ito, S. Nagai, T. Ubukata and T. Tachikawa, *CrystEngComm*, 2021, **23**, 5899; (b) S. Takahashi, S. Nagai, M. Asami and S. Ito, *Mater. Adv.*, 2020, **1**, 708; (c) S. Ito, S. Nagai, T. Ubukata, T. Ueno and H. Uekusa, *Cryst. Growth Des.*, 2020, **20**, 4443; (d) S. Ito, T. Taguchi, T. Yamada, T. Ubukata, Y. Yamaguchi and M. Asami, *RSC Adv.*, 2017, **7**, 16953; (e) S. Ito, T. Yamada, T. Taguchi, Y. Yamaguchi and M. Asami, *Chem. - Asian J.*, 2016, **11**, 1963.

11 For photophysical properties of **2**, see: (a) F. Villafiorita-Monteleone, A. Cappelli, M. Paolino, M. Colombo, E. Cariati, A. Mura, G. Bongiovanni and C. Botta, *J. Phys. Chem. C*, 2015, **119**, 18986; (b) A. Iagatti, B. Patrizi, A. Basagni, A. Marcelli, A. Alessi, S. Zanardi, R. Fusco, M. Salvalaggio, L. Bussotti and P. Foggi, *Phys. Chem. Chem. Phys.*, 2017, **19**, 13604; (c) G. He, L. Du, Y. Gong, Y. Liu, C. Yu, C. Wei and W. Z. Yuan, *ACS Omega*, 2019, **4**, 344.

12 K. E. Sapsford, L. Berti and I. L. Medintz, *Angew. Chem., Int. Ed.*, 2006, **45**, 4562.

